Thermochimica Acta 536 (2012) 30–40

Contents lists available at SciVerse ScienceDirect

Thermochimica Acta

journal homepage: www.elsevier.com/locate/tca

Kinetic study of Hubnerite ($MnWO_4$) chlorination

G.G. Fouga [a,b,c,*], R.M. Taddeo [c], M.V. Bosco [a,b], A.E. Bohé [a,b,c]

[a] Centro Atómico Bariloche Comisión Nacional de Energía Atómica, Avenida Bustillo, 9500, 8400 San Carlos de Bariloche, Argentina
[b] Consejo Nacional de Investigaciones Científicas y Técnicas (CONICET), Argentina
[c] Centro Regional Universitario Bariloche – Universidad Nacional del Comahue, 8400 San Carlos de Bariloche, Argentina

ARTICLE INFO

Article history:
Received 23 February 2011
Received in revised form 8 February 2012
Accepted 11 February 2012
Available online 23 February 2012

Keywords:
Hubnerite
$MnWO_4$
Chlorination
Kinetics
Thermogravimetry

ABSTRACT

The kinetics of Argentinean Hubnerite ($MnWO_4$) chlorination using gaseous chlorine as chlorination agent was studied between 750 and 950 °C. The relative mass change during the chlorination reaction was continuously monitored using a high resolution thermogravimetric system. The starting temperature for the reaction of the manganese tungstate with chlorine was determined at about 650 °C. The influence of gaseous flow rate, sample mass, chlorine partial pressure, and temperature on the reaction rate was analyzed. The dependence of the reaction rate with sample mass clearly indicates that the reaction is not occurring under chemical control, so the reaction proceeds under mixed control for sample masses greater than 0.5 mg. In those conditions, an apparent activation energy of 198 ± 9 kJ mol^{-1} was obtained with an isoconversional method. Concerning the influence of chlorine partial pressure, it was determined that pressures greater than 35 kPa do not modify the kinetic regime. For the experiment at 850 °C, it was found that the chlorination rate was proportional to a potential function of the partial pressure of chlorine whose exponent is around 0.85. Finally, a global rate equation that includes these parameters was developed.

1. Introduction

The increasing use of metals in modern industry leads to a gradual depletion of the primary sources of these metals. Foregoing, it led to considerable research to develop suitable methods for using low grade minerals, polymetallic minerals, industrial wastes, electronic scrap, etc. [1,2].

The efficient use of these resources requires the development of such processes to enhance the extraction of metals. Chlorination and carbochlorination are processes applied in extractive metallurgy to recovering valuable metals in the form of chlorides.

Chlorination, in the case of most of the refractory metal oxides, is one of the important intermediate steps to produce the respective metals. The raw materials for extract refractory metals are generally refractory minerals, whose decomposition requires the use of aggressive chemicals and high temperatures. It is well known that chlorine possesses a high reactivity towards many compounds at relatively low temperature. This property drove the metallurgists to use chlorine for the extraction of valuable elements from their bearing materials [3,4].

Concerning to industrial process, currently, a few metals are produced by chlorination processes. Titanium is produced by reduction of titanium tetrachloride, which is obtained by carbochlorination of natural Rutile (TiO_2), or from the so-called synthetic rutile obtained from Ilmenite ($FeTiO_3$) or from the TiO_2-rich slag produced by metallurgical treatment of Ilmenite. Zirconium is produced by fluidized-bed carbochlorination of milled Zircon sand ($ZrSiO_4$). This ore-decomposition process is used for the co extraction of hafnium because this metal is always found in zirconium ore. The chloride process is also applied to the extractive metallurgy of beryllium. At temperatures above 630 °C the components of Beryl ($Be_3Al_2Si_6O_{18}$) can be extracted in a stream of chlorine using carbon as reducing agent. These halogenides are reduced to metals with other metals or by melt electrolysis. The Kroll process is the most widely used in pyrometallurgical industrial process to produce Ti, Zr and Hf in which the metal chlorides are reduced by liquid magnesium at 800–850 °C [5].Otherwise in the literature there are reported many exploratory studies mentioning a possible future use of the chlorination process [6–9]. The use of chlorine in metal extraction process through pyro and hydrometallurgic methods has attracted considerable attention in recent decades and the use of chlorine chemistry may increase in the future. This is due to a number of factors, which include the high chlorination rates resulting from the elevated reactivity of Cl_2 and other chlorinating agents; the comparatively moderate temperature involved in the chlorination process; the low cost, variety, and availability of chlorinating agents like gaseous chlorine [7,9], carbon tetrachloride [8], hydrogen chloride [10,11], alkaline chlorides [12] and some metal chlorides [13]. Other aspects that make chlorination and carbochlorination process potentially interesting are: the favourable physical and chemical

* Corresponding author. Tel.: +54 02944 445100; fax: +54 02944 445293.
E-mail address: fouga@cab.cnea.gov.ar (G.G. Fouga).

0040-6031/$ – see front matter © 2012 Elsevier B.V. All rights reserved.
doi:10.1016/j.tca.2012.02.015

characteristics of certain metals; the properties of many chlorides (high solubility, wide variety of oxidation states, and ease of separation by liquid–liquid extraction or distillation); the selectivity of the treatment and separation processes; and the development of certain corrosion-resistant materials used for the manufacture of reactors.

With this in perspective, a thorough understanding of the kinetics of the chlorination reactions implied in a given recovery process is necessary for reactor design and to set the operation variables.

Scheelite ($CaWO_4$(s)) and Wolframite ($Fe_xMn_{1-x}WO_4$(s)) are main tungsten bearing minerals. In Argentina, there are associations formed by concentrations of these minerals in different proportions [14]. The Wolframite series consists of a complete solid solution $Fe_xMn_{1-x}WO_4$ present in nature with $0 \le x \le 1$, which is the principal source of tungsten. In the literature, there are few research works about chlorination of mixtures of these minerals. Menéndez et al. [15] analyzed the effect of Wolframite composition on its reactivity with chlorine, in the presence of sulphur dioxide. They have been working mainly with Wolframites, including a wide range of the ratio of divalent metals (Fe/Mn + Fe–WO_4(s)), and Scheelite ($CaWO_4$(s)). In a previous paper, Menéndez et al. [16] submitted a study about the main kinetic aspects of the isothermal and non-isothermal chlorination of a Scheelite ± Wolframite concentrate with chlorine and sulphur dioxide. On that occasion, they proposed a rate equation based on a diffusion mechanism with spherical symmetry, which was determined with both methods. They concluded that the control of the total kinetics corresponded to a diffusion process through the reaction products deposited on the unreacted concentrate. In other investigation, Menéndez et al. [17] determined the apparent activation energy of an isomorphous Wolframite which consisted in series of Ferberite ($FeWO_4$(s)) and Hubnerite ($MnWO_4$(s)) mixtures.

The present study is a kinetic investigation on a pure manganese Wolframite (Hubnerite $MnWO_4$(s)) arising from a reservoir of Cordoba, Argentina. This study involves the evaluation of various factors influencing on chlorination reaction kinetics, aimed to determine the mechanism of the tungsten and manganese extraction reaction in the form of halogenated compounds like chlorides or oxychlorides.

2. Experimental

2.1. Materials

The gases used were Ar(g) 99.99% purity (AGA, Argentina) and Cl_2(g) Ar 99.8% purity (INDUPA, Argentina). The solid starting material was an Argentinean pure manganese tungstate (Hubnerite: $MnWO_4$(s)) from a reservoir located in Distrito Minero Los Mogotes, Córdoba – Argentina.

2.2. Experimental equipment and procedure

2.2.1. Thermogravimetric system for non-isothermal and isothermal experiments

Mass changes occurring during Hubnerite chlorination reaction were measured using a high resolution thermogravimetric analyser (TGA). It consists of an electrobalance (model 2000, Cahn Instruments Inc.), a vertical tube furnace, a gas line, and a data acquisition system. This experimental setup has a sensitivity of ±5 μg under a gas flow rate between 2 and 8 L h^{-1} in the range of room temperature to 1000 °C.

Each sample was placed in a silica glass crucible, which hangs from one of the arms of the electrobalance through a silica glass wire. A silica glass hang down tube carried the gases to the sample. The temperature of the sample was measured using a Pt–Pt (10%Rh) thermocouple encapsulated in silica glass, which was placed 2 mm below the crucible. Flows of Ar(g) and Cl_2(g) gases were controlled by means of flowmeters. Non-isothermal and isothermal runs were performed. In both cases, samples were placed in a cylindrical silica glass crucible (diameter = 0.72 cm, high = 0.42 cm). The samples were well spread in the crucible forming a thin layer. Before reaching the selected reaction temperature for each experiment, the samples were heated to 100 °C in Ar(g) flow in order to remove water. In non-isothermal runs, the Cl_2(g) was introduced and the samples were heated in the resulting mixture Cl_2(g)–Ar(g) (P_{Cl_2} = 35 kPa) to 950 °C. A linear heating rate of 5.3 °C min^{-1} was used. Relative mass changes monitored were acquired every 3 s using a data acquisition system with the experimental setup described above.

From these measurements, it was determined the experimental mass change as $\Delta M = m_0 - m_t$, where m_0 and m_t are the initial mass and the mass at time t, respectively.

According to the following equation:

$$MnWO_4(s) + Cl_2(g) \rightarrow MnCl_x(g) + WO_xCl_y(g) \quad (1)$$

If the manganese chloride and tungsten oxychloride are gaseous species the conversion degree (α) can be defined by $\Delta M/m_0$.

Usually, the rate of a heterogeneous solid–gas reaction can be written, assuming separability of variables [18], as:

$$\text{Rate} = \frac{d\alpha}{dt} = F(\alpha) \cdot K(T) \cdot F(P_{Cl_2}) \quad (2)$$

In Eq. (2) $F(\alpha)$ is a function that describes the geometric evolution of the reacting solid, $K(T)$ refers to an Arrhenius equation, and $F(P_{Cl_2})$ expresses the dependence of the reaction rate on the chlorine partial pressure. This mathematical procedure allows to exclude mass sample effects and represents an appropriate approach for gas–solid reaction analysis.

2.2.2. Fixed bed reactor for isothermal experiments

A fixed bed reactor was employed in order to determine the chlorination reaction stoichiometry and to analyse the reaction products. A schematic diagram of the reactor device is shown in Fig. 1. This reactor is a silica glass tube where the sample was introduced using a silica glass crucible. The temperature of the hot zone (zone A) was maintained by a furnace. Zones B and C correspond to the cold part of the reactor where volatile species were condensed. The chlorine gas was introduced when the system reaches the working temperature. At the end of each run, the reactant gas was cut off and argon stream was introduced to purge the reactor.

3. Thermodynamic considerations

The first step of this study was the calculation of standard free energy changes of the probable reaction considered in the present work. The thermodynamic calculations for the Hubnerite chlorination reactions were performed using HSC chemistry for windows software [19].

In the literature, there are reported several manganese chlorides: MnCl(g), $MnCl_2$(s,l,g), $MnCl_3$(s,l,g), $MnCl_4$(l,g) and Mn_2Cl_4(g) [19,20]. In a previous research, the authors reported the formation of $MnCl_2$(s,l,g) as stable phase for the direct chlorination reaction of MnO(s), Mn_3O_4(s) and Mn_2O_3(s) [21]. Therefore, the $MnCl_2$(s,l,g) was considered as the stable phase formed, which leads to manganese content elimination through volatilization at temperatures above 650 °C. Moreover, the compounds reported for tungsten are: WCl(g), WCl_2(s,l), WCl_3(s,l,g), WCl_4(s,l,g), WCl_5(s,l,g), WCl_6(s,l,g), W_2Cl_{10}(g), WOCl(g), $WOCl_2$(s,l), $WOCl_3$(s,l,g), $WOCl_4$(s,l,g), WO_2Cl(s,g), WO_2Cl_2(s,l,g), and physicochemical properties are shown in Table 1 [19,20].

The $MnWO_4$(s)–Cl_2(g) reaction can involve the formation of several reaction products, according to Eqs. (3)–(15). These equations

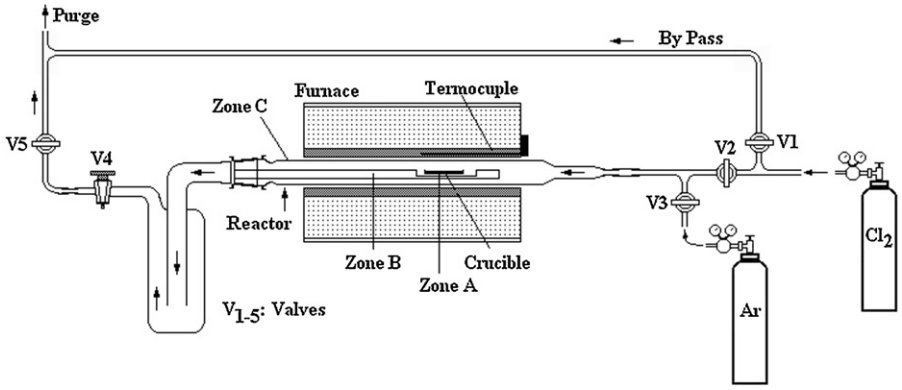

Fig. 1. Schematic diagram of fixed bed reactor.

show the possible Hubnerite chlorination reaction stoichiometry, which foresee the formation of $MnCl_2$(s,l,g) and tungsten chlorides or oxychlorides.

$$2/3MnWO_4(s) + Cl_2(g) \rightarrow 2/3MnCl_2(s,l,g) + 2/3WCl(g) + 4/3O_2(g) \quad (3)$$

$$1/2MnWO_4(s) + Cl_2(g) \rightarrow 1/2MnCl_2(s,l,g) + 1/2WCl_2(s,l,g) + O_2(g) \quad (4)$$

$$2/5MnWO_4(s) + Cl_2(g) \rightarrow 2/5MnCl_2(s,l,g) + 2/5WCl_3(s,g) + 4/5O_2(g) \quad (5)$$

$$1/3MnWO_4(s) + Cl_2(g) \rightarrow 1/3MnCl_2(s,l,g) + 1/3WCl_4(s,l) + 2/3O_2(g) \quad (6)$$

$$2/7MnWO_4(s) + Cl_2(g) \rightarrow 2/7MnCl_2(s,l,g) + 2/7WCl_5(s,l,g) + 4/7O_2(g) \quad (7)$$

$$1/4MnWO_4(s) + Cl_2(g) \rightarrow 1/4MnCl_2(s,l,g) + 1/4WCl_6(s,l,g) + 1/2O_2(g) \quad (8)$$

$$2/7MnWO_4(s) + Cl_2(g) \rightarrow 2/7MnCl_2(s,l,g) + 1/7W2Cl_{10}(g) + 4/7O_2(g) \quad (9)$$

$$2/3MnWO_4(s) + Cl_2(g) \rightarrow 2/3MnCl_2(s,l,g) + 2/3WOCl(g) + O_2(g) \quad (10)$$

$$1/2MnWO_4(s) + Cl_2(g) \rightarrow 1/2MnCl_2(s,l,g) + 1/2WOCl_2(s,l) + 3/4O_2(g) \quad (11)$$

$$2/5MnWO_4(s) + Cl_2(g) \rightarrow 2/5MnCl_2(s,l,g) + 2/5WOCl_3(s,l,g) + 3/5O_2(g) \quad (12)$$

$$1/3MnWO_4(s) + Cl_2(g) \rightarrow 1/3MnCl_2(s,l,g) + 1/3WOCl_4(s,l,g) + 1/2O_2(g) \quad (13)$$

$$2/3MnWO_4(s) + Cl_2(g) \rightarrow 2/3MnCl_2(s,l,g) + 2/3WO_2Cl(s) + 2/3O_2(g) \quad (14)$$

$$1/2MnWO_4(s) + Cl_2(g) \rightarrow 1/2MnCl_2(s,l,g) + 1/2WO_2Cl_2(s,l,g) + 1/2O_2(g) \quad (15)$$

Table 1
Physicochemical properties of tungsten and manganese compounds.

	Melting point (°C)	Boiling point (°C)
W compounds		
Oxides		
WO(s)	Not reported	Not reported
WO_2(s)	1723.85	1500 (dec)
WO_3(s)	1472	1837
Chlorides		
WCl(g)	Not reported	Not reported
WCl_2(s,l,g)	588.85	926.85
WCl_3(s,g)	550 (dec)	806[a]
WCl_4(s,l)	498	Not reported
WCl_5(s,l,g)	242	286
WCl_6(s,l,g)	275	346.75
W_2Cl_{10}(g)	Not reported	Not reported
Oxychlorides		
WOCl(g)	Not reported	Not reported
$WOCl_2$(s,l)	Not reported	Not reported
$WOCl_3$(s,l,g)	Not reported	Not reported
$WOCl_4$(s,l,g)	211	227.55
WO_2Cl(s,g)	Not reported	Not reported
WO_2Cl_2(s,g)	264.85	472[a]
Mn compounds		
Chlorides		
MnCl(g)	Not reported	Not reported
$MnCl_2$(s,l,g)	650	1190
$MnCl_3$(s,l,g)	587	627
$MnCl_4$(l,g)	Not reported	Not reported
Mn_2Cl_4(g)	Not reported	Not reported
Oxides		
MnO(s,g)	1842	3127
MnO_2(s,g)	535 (dec)	Not reported
Mn_2O_3(s)	1347	Not reported
Mn_3O_4(s)	1562	Not reported
Oxychlorides		
$MnClO_3$(g)	Not reported	Not reported

[a] Calculated with Software HSC 6.12 chemistry.

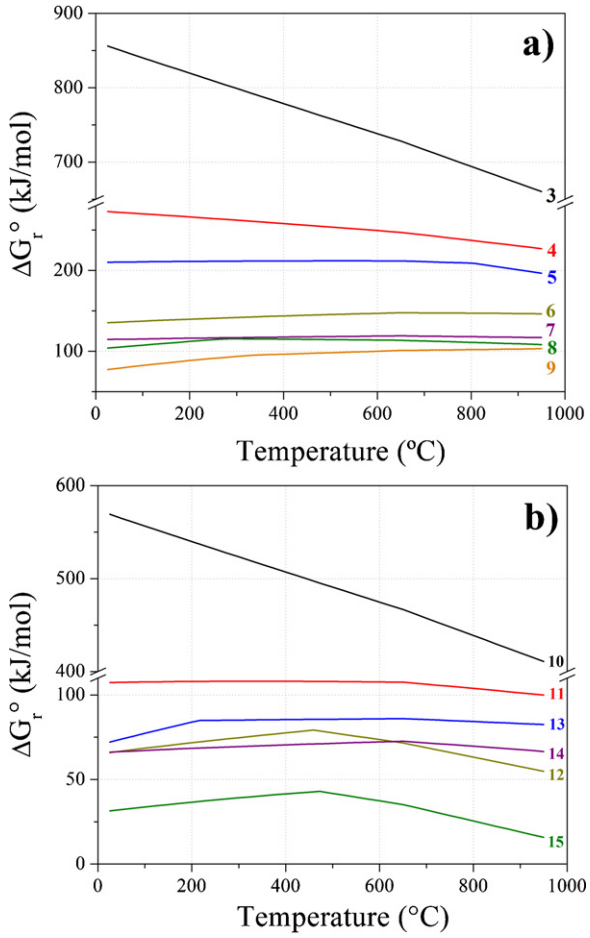

Fig. 2. Ellingham diagram for the Hubnerite chlorination reaction: (a) showing the formation of different tungsten chlorides; (b) showing the formation of different tungsten oxychlorides.

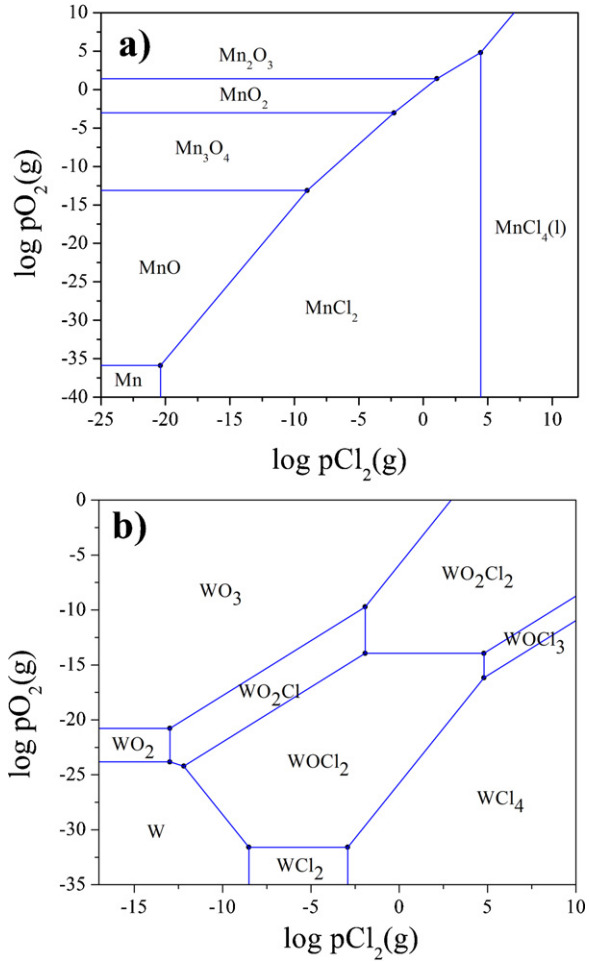

Fig. 3. (a) Phase stability diagram for Mn—Cl—O system at 650 °C, and (b) phase stability diagram for W—Cl—O system at 650 °C.

Fig. 2(a) and (b) shows the Ellingham diagram for Eqs. (3)–(15). They summarize the evolution of standard free energy changes per mol of chlorine, ΔG_r°, as a function of temperature. The positive values of ΔG_r°, for all the reactions considered before, are indicating that they are thermodynamically unfavourable. Moreover, the equations that include the formation of different tungsten oxychlorides are those with the lowest ΔG_r° values. As can be seen in Table 2, the values of the equilibrium constants show that, above 750 °C, the reactions given by Eqs. (12)–(15) would occur with the formation of gaseous tungsten oxychlorides species and liquid manganese chloride. The low equilibrium constant values are indicating that the reactions will not attain the complete conversion. Nevertheless, in our experimental setup where the chlorinations were carried out in a continuous chlorine flow, the removal of volatile products would assure to reach the complete conversion.

Table 2
Equilibrium constant for Eqs. (10)–(15), as a function of temperature.

Eq.	*K*		
	750 °C	850 °C	950 °C
(10)	1.403×10^{-23}	1.115×10^{-20}	2.949×10^{-18}
(11)	3.349×10^{-39}	5.415×10^{-36}	2.516×10^{-33}
(12)	4.246×10^{-4}	0.00155	0.00456
(13)	4.745×10^{-5}	1.306×10^{-4}	3.047×10^{-4}
(14)	2.484×10^{-4}	6.454×10^{-4}	0.00144
(15)	0.03427	0.09259	0.2125

Fig. 3 shows the phase stability diagram for: (a) Mn—Cl—O; and (b) W—Cl—O systems at 650 °C. At the beginning of the chlorination, the values of partial pressure of $Cl_2(g)$ was 0.35 atm and the oxygen was below 10^{-4} atm. The $O_2(g)$ is present in the argon as an impurity.

As can be seen $MnCl_2(l)$ can be formed under the experimental conditions. At this temperature, the $MnCl_2(l)$ vapour pressure is 2.77×10^{-4} atm. so, it is possible to observe mass loss by volatilization. Furthermore, as can be seen in Fig. 3b, for these experimental conditions (pCl_2 = 0.35 atm and pO_2 below 10^{-4} atm), for the W—Cl—O systems the possible stable phases are WO_2Cl, WO_2Cl_2, $WOCl_2$ and $WOCl_3$.

4. Results and discussion

4.1. Hubnerite characterization

Structures of the starting sample, as well as the condensed phases and chlorination reaction residues, were well characterized by Scanning Electron Microscopy (SEM 515, Philips XL30 Electronics Instruments) and X-ray diffraction (XRD, Philips PW1310/01), with Ni filtered Cu Kα radiation. Multielement analysis was carried out by Energy Dispersive X-Ray Fluorescence Spectroscopy (ED-XRF, Shimadzu, EDX 800 HS).

Before analyses, the sample was pulverized using a micronized mill grinding. Analysis of powder samples was performed to find the particle size and size distribution by laser diffraction

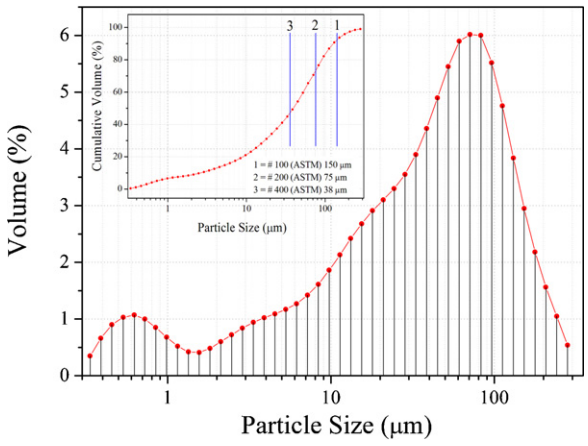

Fig. 4. Histogram of particle size distribution.

(Mastersizer Micro). A histogram of particle size distribution is shown in Fig. 4. Through the volumetric percent analysis, it was determined that about 50% corresponds to particles which granulometry is below 38 μm (#400 ASTM). The remaining percentages of the sample has the following size distribution: 20% between 38 and 75 μm (#400–#200 ASTM), 25% between 75 and 150 μm (#200–#100 ASTM) and the 5% of the sample corresponds to particles which granulometry is greater than 150 μm (#100 ASTM).

Fig. 5 shows the diffractogram of the starting sample with the reference pattern. By comparing the positions and intensities of the diffraction peaks, it can be concluded that the starting sample is composed by a simple phase of $MnWO_4$(s) which crystallizes in the monoclinic system (space group P2/c). Fig. 6 shows SEM images of this sample. Fig. 6(a) shows the average particle sizes mostly found in the fraction of sample investigated in this work.

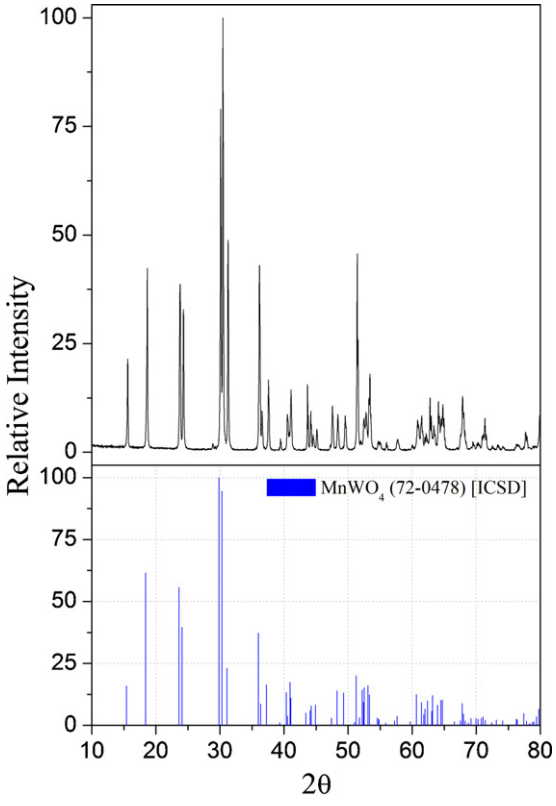

Fig. 5. XRD analysis of starting sample.

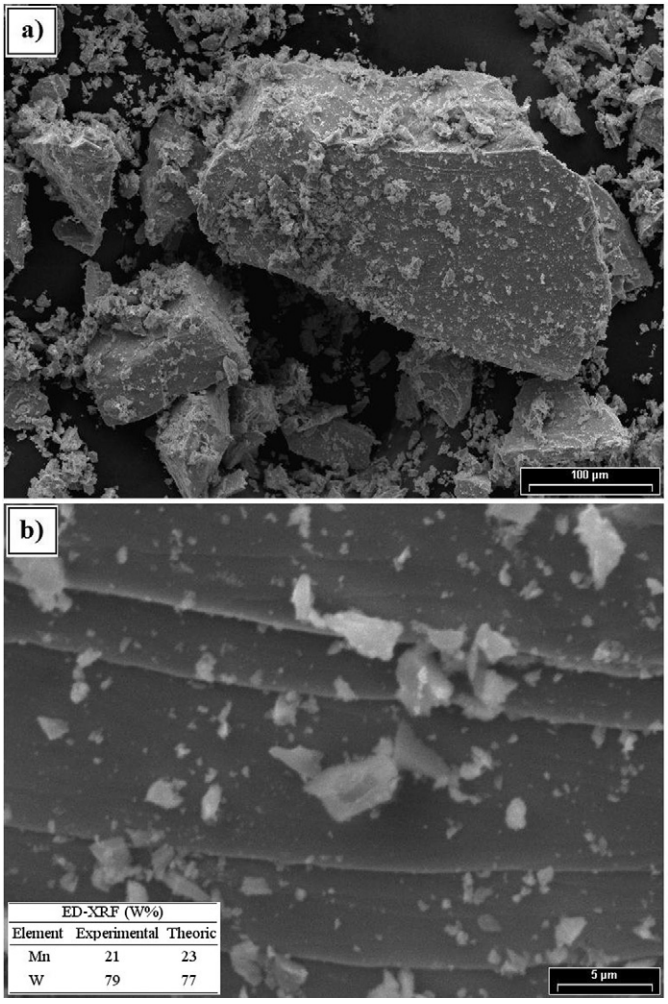

Fig. 6. SEM images and ED-XRF analysis of initial sample.

No porosity can be observed in the sample surfaces, Fig. 6(b). Multielement analysis carried out by ED-XRF, shows that the sample is composed by W—Mn with a good concordance with the $MnWO_4$(s) stoichiometry.

4.2. Non-isothermal chlorination reaction

The starting temperature for the Hubnerite chlorination was determined by non-isothermal thermogravimetric measurements. The experimental conditions were: a linear heating rate of 5.3 °C min^{-1}; Cl_2(g)–Ar(g) flow = 4 L h^{-1}, m_0 = 10 mg and P_{Cl_2} = 35 kPa.

In Fig. 7 the ratio between the mass change and initial sample mass as a function of temperature is shown. The reaction starts at approximately 650 °C, where the sample commences to lose mass, denoting the formation of gaseous products.

In order to confirm that the gaseous chlorine break the bounds in the Hubnerite structure, the reaction was interrupted at 850 °C and the solid residue was analysed by X-ray diffraction. The diffractogram shows that only unreacted Hubnerite remains in the crucible. Meanwhile, the manganese and tungsten have formed the respective volatile chloride and oxychloride which were dragged by the gas stream. This continuous mass loss is due to the removal of two possible compounds, manganese as $MnCl_2$(g) [21] which has a vapour pressure of 2.77×10^{-4} atm. at 650 °C and tungsten as any oxychloride with high enough vapour pressure [19].

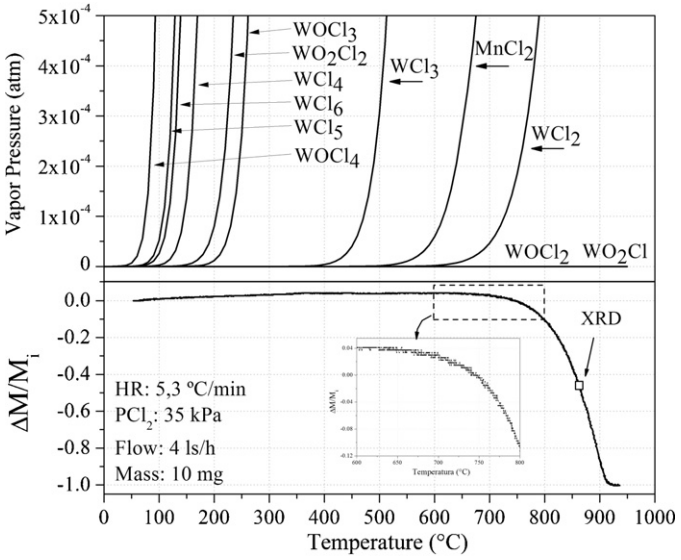

Fig. 7. Non-isothermal chlorination reaction.

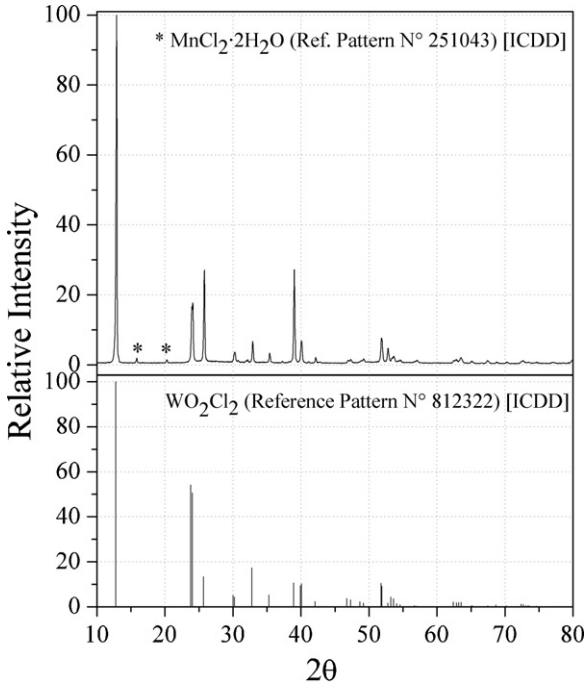

Fig. 8. X-ray diffractogram of chlorination product.

4.3. Isothermal chlorination reactions

4.3.1. Chlorination in the fixed bed reactor

In order to identify the $MnWO_4$ chlorination reaction products, experiments were conducted in fixed the bed reactor shown in Fig. 1. The experimental conditions were: $T = 950\,^{\circ}C$; $P_{Cl_2}(g) = 1$ atm; $Cl_2(g)$ flow = $2\,L\,h^{-1}$; $m_0 = 500$ mg. Through the analysis of the chlorination reaction products from the fixed bed reactor, it was confirmed that the manganese content was removed as $MnCl_2(g)$ (Rhombohedral SG: R-3 m), which then was hydrated to form $MnCl_2{\cdot}2H_2O(s)$ (Monoclinic SG: C2/m). Moreover, the tungsten was removed by the formation and subsequent evaporation of $WO_2Cl_2(g)$ (Orthorhombic SG: Immm), according to the reaction given by Eq. (15). This stoichiometry was observed in all temperature range studied. Manganese chlorides and tungsten oxychloride were collected in the so called cold zone (zones *B* and *C* in the scheme shown in Fig. 1).

The chlorination products were characterized by SEM and X-ray diffraction. XRD pattern obtained is showing in Fig. 8 where a good agreement is achieved with the corresponding reference patterns for the tungsten IV oxychloride [22] also shown in the figure.

Fig. 9 shows SEM images of condensed tungsten oxychloride. The microscopic morphology of $WO_2Cl_2(s)$ consists of intergrowth crystals of different sizes ranging between 10 and 50 μm, mainly in the form of rectangular plates. Fig. 10 shows SEM images of condensed $MnCl_2(s)$. It can be seen that the manganese chloride morphology is so different, revealing high porosity agglomerates constituted by interconnected particles; these characteristic corresponds to the fact that the metallic chloride is very hygroscopic.

4.3.2. Thermogravimetric experiments

4.3.2.1. Analysis of mass transfer in the gaseous phase. In order to determine the intrinsic kinetic parameters of a heterogeneous reaction, the effects of mass transfer should be firstly disregarded. The mass transfer phenomena in the gaseous phase that could affect the kinetic regimen are two: "exhaustion of the reagent gas" and "diffusion through the boundary layer surrounding the solid sample".

4.3.2.1.1. Reagent gas starvation. In order to assess whether the system is on exhaustion of the reagent gas condition (starvation), the influence of the $Cl_2(g)$–Ar(g) flow over the reaction rate was analyzed. Gas starvation occurs when the flow is low. Then, the overall rate of reaction is linearly dependent of the gas flow. The study of this phenomena is performed by increasing the gas flow and determining its influence on the reaction rate [23]. For a specific flow value, there are no more changes when increasing the gaseous flow; thus, it can be assumed that the system is not starved of gaseous reactant. In order to determine this condition, the influence of $Cl_2(g)$–Ar(g) flow was analysed.

Fig. 11(a) and (b) illustrates the effects of chlorine flow rate on the chlorination of $MnWO_4$ at 950 °C and 850 °C, respectively. Experiments were performed at four different flow rates: 2, 4, 6, and $8\,L\,h^{-1}$, which is the maximum flow rate that the experimental system can reach, while the partial pressure of chlorine was kept constant at 35 kPa. The sample mass used was 2 mg. In Fig. 11(a), the behaviour observed at 950 °C is shown. It can be appreciated that, when the chlorine flow rate was increased, the rate of mass loss observed to be faster. For instance, a conversion of 0.5 was achieved in about 186, 172, 134 and 114 s for flow rates of 2, 4, 6 and $8\,L\,h^{-1}$, respectively. Then, it can be concluded that chlorination rate increases with increasing the flow rate, and thus, the rate-controlling regime at 950 °C depends on the mass transfer in the gaseous phase outside from the boundary layer.

Fig. 11(b) shows the effect of chlorine flow rate at 850 °C. A conversion of 0.5 was achieved in approximately 907 s for $2\,L\,h^{-1}$, indicating a significant decrease in the chlorination rate with temperature reduction. Therefore, the intrinsic reactivity of the solid is strongly affected by the temperature. When the flow rate was increased from 4 to $8\,L\,h^{-1}$, it was seen that the reaction rate did not depend on the $Cl_2(g)$–Ar(g) flow, because it was nearly constant and the obtained values were located within the experimental uncertainty.

As discussed by Hills [24], when variations in the flow rate of the reacting gas do not produce significant changes in the reaction rate, it may be concluded that reacting gas starvation is absent. Hence, the experimental results shown in Fig. 11(b) enable to conclude that the rate of chlorine supply above $4\,L\,h^{-1}$ is high enough for avoiding starvation effects in Hubnerite ($MnWO_4(s)$) chlorination at 850 °C and lower temperatures.

The next step in the present analysis is to determine if the reaction rate is in the order of the gaseous reactive diffusion process

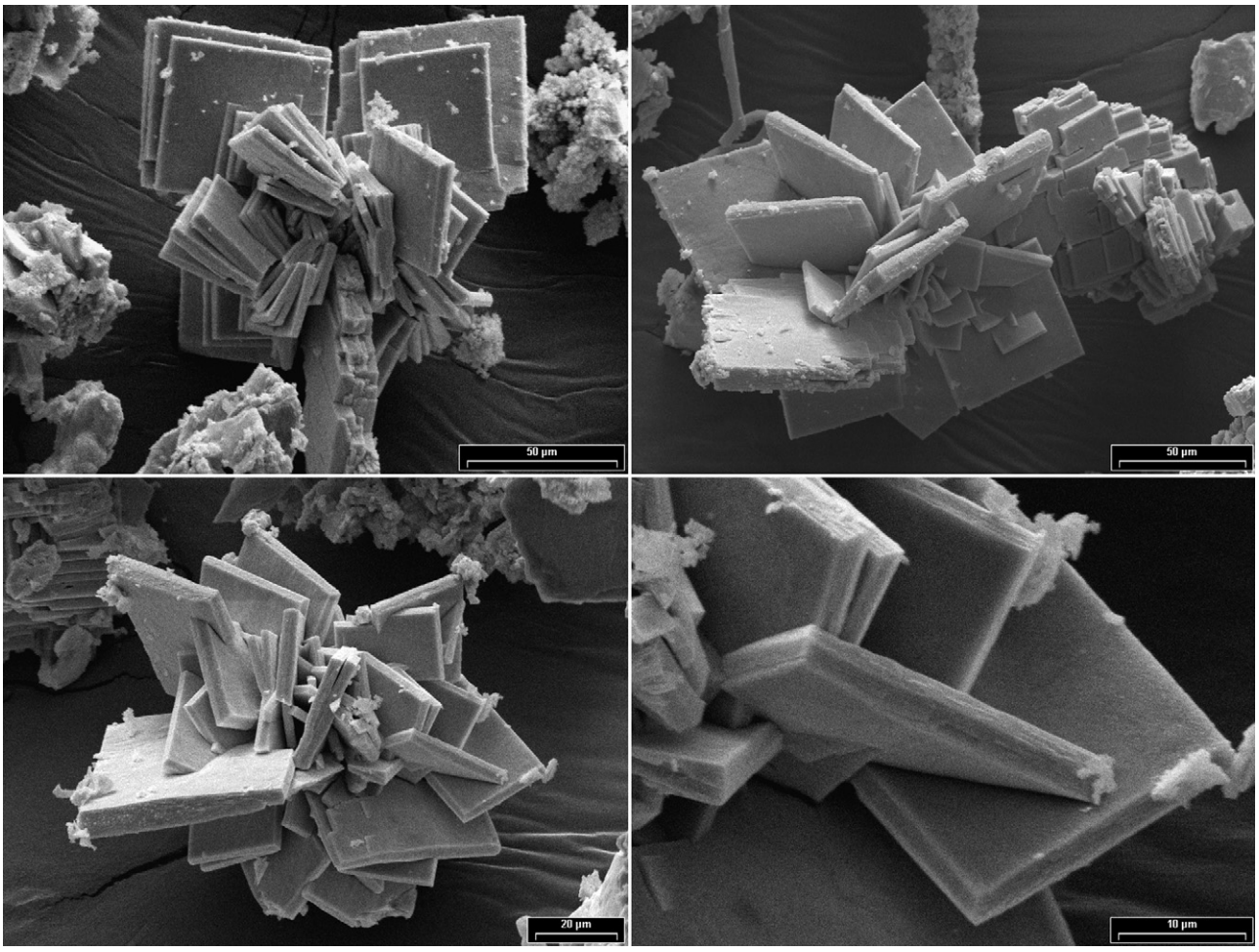

Fig. 9. SEM images of condensed WO_2Cl_2(s).

through the boundary layer. The procedure used to define if the reaction rate is controlled by the diffusion through the boundary layer is extensively explained in the following section.

4.3.2.1.2. Diffusion through the boundary layer surrounding the solid sample. Another process that can influence the chlorination rate is the mass transfer through the boundary layer surrounding the solid sample, even using a gas flow high enough for avoiding the starvation of the reagent gas. As reported by several authors [23,25], mass transfer into the gas boundary layer surrounding solid samples may play an important role in controlling the reaction rate.

For a reaction such as that expressed by Eq. (1), the Cl_2(g) molar transfer rate from the gas stream to the solid surface (N) is given by the following equation [23]:

$$N = A \cdot \frac{h_d}{R \cdot T} \cdot (P^B_{Cl_2} - P^S_{Cl_2}) \tag{16}$$

where A is the external area of the reactive solid; h_d is the mass transfer coefficient (boundary layer resistance); R is the universal gas constant; T is the temperature in K; and $P^B_{Cl_2}$ and $P^S_{Cl_2}$ are the Cl_2(g) concentrations in the gas stream and in the solid surface, respectively, expressed as partial pressures.

The value of the mass transfer coefficient (h_d) depends on many factors, such as the relative rate between the particle and fluid, particle size and fluid properties. These factors have been correlated for various types of solid–fluid contact. An equation that takes into account all these factors is the well known Ranz–Marshall correlation (RzM) of the molar gaseous reactive flux [25]:

$$N = \frac{D_{Cl_2\text{–}Ar} \cdot (2.0 + 0.6Re^{1/2}Sc^{1/3}) \cdot (P^B_{Cl_2} - P^S_{Cl_2}) \cdot A}{R \cdot T \cdot l} \tag{17}$$

where N refers to the molar flow of chlorine; D is the diffusion coefficient for chlorine diffusing through argon; $Re = U \cdot l/\nu$ and $Sc = \nu/D$ are the Reynolds and Schmidt numbers, respectively (U is the linear fluid velocity and ν is the kinematic viscosity); $P^B_{Cl_2}$ and $P^S_{Cl_2}$ are the Cl_2(g) partial pressures in the gas stream and solid surface, respectively; A is the sample external surface (crucible area = 0.43 cm^2); and l is the sample characteristic dimension (crucible diameter = 0.74 cm).

Table 3 shows the values of N for $P_{Cl_2} = 35$ kPa, Cl_2(g)–Ar(g) flow = 4 L h^{-1}, and several temperatures, as calculated by Eq. (17). The values of $D_{Cl_2\text{–}Ar}$ (binary diffusion coefficient) and ν (kinematic viscosity), were obtained from the Chapman/Enskog theory [23,26].

For these gasses in the temperature range between 750 °C and 950 °C, the binary diffusion coefficient can be expressed by: $D_{Cl_2\text{–}Ar} = -0.35 + 1.8 \times 10^{-3}\,T$ ($cm^2\ s^{-1}$).

The values obtained by using Eq. (17) are only approximate, because this equation is valid for a pellet in a freely flowing gas and not for a sample contained within a crucible. Hills [24] and Hakvoort [27] concluded that the values given by Eq. (17) are more than one order of magnitude higher than the mass transfer rates corresponding to powders contained within crucibles.

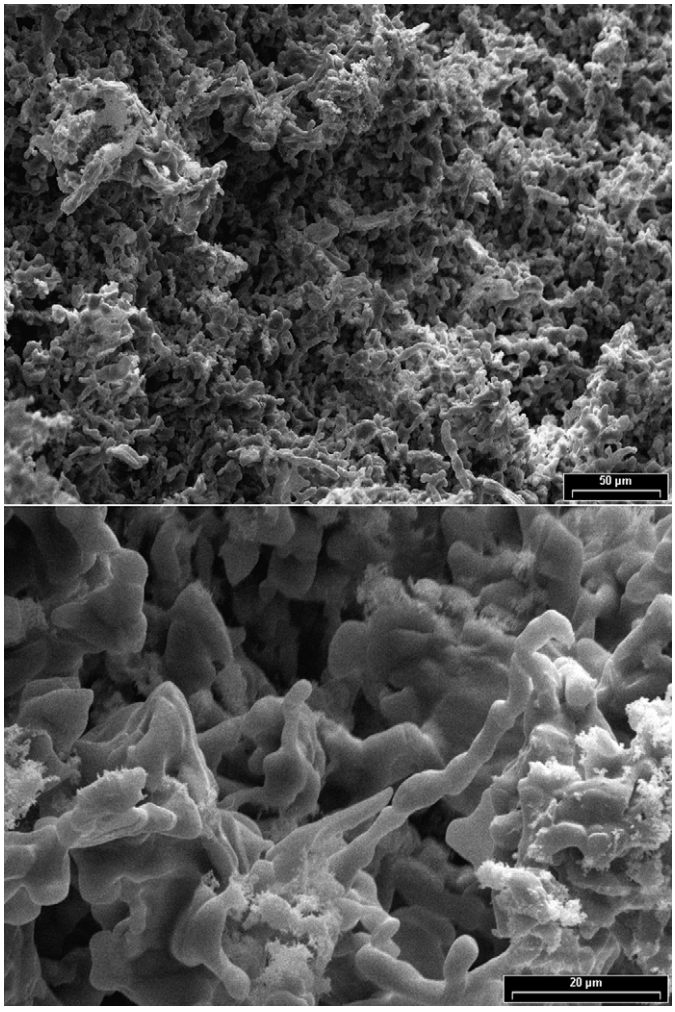

Fig. 10. SEM Images of condensed $MnCl_2$(s).

Table 3
Theoretical and experimental Cl_2(g) molar transfer rates.

Temperature (°C)	Cl_2(g) molar transfer rate (mol s^{-1})		N_T/N_E
	N_T theoretical[a]	N_E experimental[b]	
750	1.46×10^{-06}	9.47×10^{-10}	1542
775	1.49×10^{-06}	1.41×10^{-09}	1057
800	1.51×10^{-06}	2.41×10^{-09}	627
825	1.54×10^{-06}	3.83×10^{-09}	402
850	1.56×10^{-06}	7.26×10^{-09}	215

Conditions used for the calculation: $l = 0.74$ cm, $A = 0.43$ cm^2, $P_{Cl_2} = 35$ kPa, and Cl_2(g)–Ar(g) flow = 4 L h^{-1}.
[a] Calculated from Eq. (17).
[b] Obtained from the lineal range of the thermogravimetric curves.

Using this approximation, the comparison between the theoretical rate values given by Eq. (17) with those obtained from experimental measurements permits to determine whether the reaction is under mass transfer control through the boundary layer [28,29]. When the experimental rate is in the order of the calculated value it can be concluded that the reaction is under mass transfer control. On the opposite, when the experimental rate is two or more orders of magnitude smaller than the calculated value, the reaction may be in mixed control or in pure chemical control. In the case of reaction under diffusion control, the interfacial reaction rate will be so fast, that the reaction rate will be controlled by diffusion through the boundary layer and then, the values of N will tend to the theoretical value. For these reason, the experimental values cannot be greater than the calculated values.

As it can be seen in Table 3, the experimental rates at 850 °C and lower temperatures are three or more orders of magnitude smaller than the RzM calculated rates. These results are indicating that, at temperatures below 850 °C, the convective mass transfer through the boundary layer is not the rate-controlling step.

4.3.2.2. Analysis of mass transfer through the sample pores. In order to analyze the influence of sample mass on the Hubnerite chlorination reaction rate, chlorination reactions were performed with different sample masses. The experimental conditions were: $T = 850$ °C; $P_{Cl_2} = 35$ kPa and Cl_2(g)–Ar(g) flow = 4 L h^{-1}. The corresponding TG curves with the reaction degree as a function of time, are depicted in Fig. 12. It can be seen that the reaction rate measured as $d\alpha/dt$, becomes faster as the sample mass decreases from 40 to 0.5 mg. The times to achieve 50% of the reaction ($t_{\alpha=0.5}$) are: 4220, 3524, 2165, 1230, 771, 431 and 245 s for 40, 20, 10, 5, 2.5, 1 and 0.5 mg respectively. Nevertheless, this behaviour is different to those reactions under chemical control where the reaction

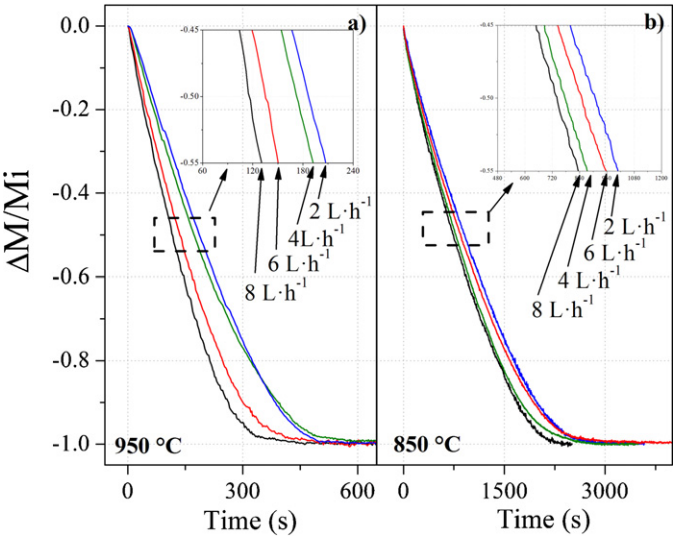

Fig. 11. Effect of chlorine flow rate on the chlorination of $MnWO_4$(s) at two temperatures.

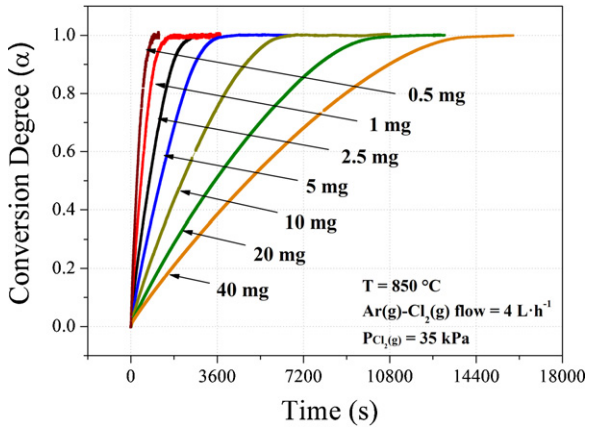

Fig. 12. Influence of sample mass on the Hubnerite chlorination reaction rate.

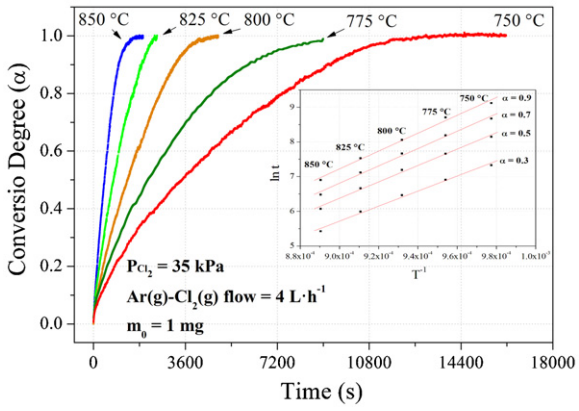

Fig. 13. TG curves for the chlorination of 1 mg of Hubnerite at different temperatures. Right inset plot shows linear fit obtained from Eq. (22).

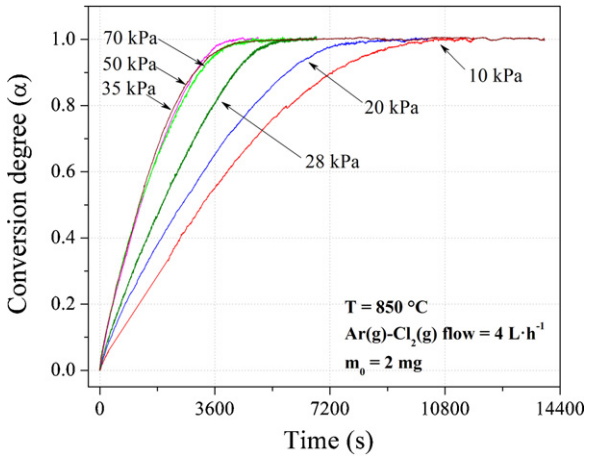

Fig. 14. Effect of chlorine partial pressure on the Hubnerite chlorination rate.

rate measured as $d\alpha/dt$ has a constant value, meaning that the time required to reach $\alpha = 0.5$ is the same for all masses studied [28–30].

Therefore, the dependence of the reaction rate with the sample mass found in the experiments is clearly indicating that, at 850 °C, the reaction is not occurring under chemical control. At 750 °C the same dependence with sample mass was observed. Possible process controls compatible with the behaviour observed are: mass transfer through the boundary layer surrounding the solid sample (mass transfer in the gas phase) and pore diffusion coupled with chemical reaction (mixed control). As it was previously demonstrated that the mass transfer in the gas phase is not the reaction control process, it can be concluded that the $MnWO_4$(s) chlorination reactions, at 850 °C, proceed under mixed control. In order to analyze the effect of temperature and chlorine partial pressure on the Hubnerite chlorination rates, samples less than 2.5 mg were used for further experiments, because they showed good reproducibility.

4.3.2.3. Analysis of the temperature effects. Fig. 13 shows α–t curves for Hubnerite ($MnWO_4$(s)) chlorination between 750 and 850 °C. The experimental conditions were: $P_{Cl_2} = 35$ kPa; Cl_2(g)–Ar(g) flow = 4 L h^{-1}, and initial mass = 1 mg. It can be seen a strong dependence of the chlorination rate with temperature: the reaction is faster as temperature increases.

As expressed earlier, the rate of a heterogeneous solid–gas reaction can be expressed by Eq. (4). The activation energy (Ea) included in the Arrhenius type equation for $K(T)$ can be calculated from this expression, even if functions $F(P_{Cl_2})$ and $F(\alpha)$ are unknown, by applying a "model-free" method [31,32]. The analysis of Ea at different conversion degrees allows to determine if there is a change rate controlling mechanism during the reaction.

By rearranging Eq. (2) and integrating:

$$\int_0^{\alpha_i} \frac{d\alpha}{F(\alpha)} = f(\alpha_i) = \int_0^{t_i} K(T)\cdot F(P)\cdot dt \tag{18}$$

$$f(\alpha_i) = K(T)\cdot F(P)\cdot t_i \tag{19}$$

Assuming that $K(T)$ follows an Arrhenius form, rearranging and applying natural logarithms:

$$f(\alpha_i) = k_0\cdot e^{-Ea/R\cdot T}\cdot F(P)\cdot t_i \tag{20}$$

$$\ln\ t_i = \ln\left[\frac{f(\alpha_i)}{F(P)\cdot k_0}\right] + \frac{E_a}{RT} \tag{21}$$

for a given α_i:

$$\ln\ t_i = cte + \left(\frac{E_a}{R}\right)\cdot\frac{1}{T} \tag{22}$$

The first term on the right-hand side of Eq. (22), the constant, is a function of the reaction degree and chlorine partial pressure. Therefore, if the chlorine partial pressure remains constant, and the time to attain a certain reaction degree is determined as a function of temperature, Eq. (22) allows to obtain the activation energy from the slope of the plot $\ln t_i$ vs. T^{-1}. The values of time necessary to calculate $\ln t$ were obtained from the curves of α vs. t at different temperatures (Fig. 13). The graphical representation of these results are shown in the inset plot in Fig. 13 for $\alpha = 0.3$, 0.5, 0.7 and 0.9. An apparent activation energy of 198 ± 9 kJ mol^{-1} was determined from the slope of the linear regression. The constant value of Ea, obtained as a function of the reaction degree within the temperature range, suggests that the rate controlling step does not change during the total reaction.

4.3.2.4. Analysis of the chlorine partial pressure effect. In order to evaluate the effect of chlorine partial pressure on the Hubnerite chlorination rate, experiments were performed at 850 °C and different Cl_2(g) partial pressures. The experimental conditions were: Cl_2(g)–Ar(g) flow = 4 L h^{-1}; and $m_0 = 2$ mg.

Fig. 14 shows α–t curves for Hubnerite chlorination in the P_{Cl_2} range between 10 and 70 kPa. As it can be seen, the reaction becomes faster as chlorine partial pressure increases from 10 to 35 kPa. The times to achieve 50% of the reaction ($t_{\alpha=0.5}$) were: 3200, 2572, and 1940 s for 10, 20 and 28 kPa respectively. For pressures higher than 35 kPa, the chlorination rate is unaffected. The time to achieve 50% of the reaction ($t_{\alpha=0.5}$) for 35, 50, and 70 kPa was 1255 s.

To calculate the reaction order of the reaction with respect to P_{Cl_2}, the procedure applied was analogous to that used to determine Ea. Eq. (2) was integrated, $F(P_{Cl_2})$ was assumed of the form of $B\cdot P_{Cl_2}^x$ (where B is a constant and x is the reaction order with respect to the chlorine partial pressure, for reactions where the overall rate is controlled by chemical kinetic). For a constant temperature and applying natural logarithms, the following expression was obtained:

$$-\ln\ t_i = H(\alpha_i) + x\cdot\ln P_{Cl_2} \tag{23}$$

where t_i is the time at which a conversion degree α is obtained at a temperature T; and $H(\alpha)$ is a function that depends on α (since T is kept constant). From the slope of the straight lines of the $-\ln t_i$ vs. $P_{Cl_2(g)}$ plot for different conversion degrees. At 850 °C, it was found that the chlorination rate was proportional to a potential function of the partial pressure of chlorine whose exponent x is around 0.85.

Table 4
Apparent rate constant k and fittings correlation coefficient, obtained from fitting experimental data with the sphere contractile kinetic model $(1-(1-\alpha)^{1/3} = k \cdot t)$.

Temperature (°C)	k (s^{-1})	Correlation coefficient
850	5.09×10^{-4}	0.99834
825	2.58×10^{-4}	0.99932
800	1.49×10^{-4}	0.99893
775	8.35×10^{-5}	0.99975
750	5.14×10^{-5}	0.99940

4.4. A proposed kinetic equation for Hubnerite chlorination

When there is not a solid residue formation as in the case of chlorination reactions producing high vapour pressure chlorides, the reactive particle decreases in size during the course of the reaction until its total disappearance. From the experimental thermogravimetric curves, the α_t values were obtained. The experimental conversion vs. time curves were fitted with the following conversion function that describes a reaction proceeding according to a topochemically contracting geometry [23,33,34]:

$$f(\alpha) = 1 - (1-\alpha)^{1/n} = k \cdot t \tag{24}$$

where α is the fractional conversion, and the value of n depends on the solid geometry, being 1, 2, or 3 for slabs, cylinders, and spheres, respectively.

Analyzing the correlation coefficient of the fittings of these models, it was found that the contractile sphere model achieved the best fit. The values of the apparent rate constant k, obtained for the different temperatures, are shown in Table 4 together with the correlation coefficient of the fittings. As it can be seen, the contractile sphere model gives a good description of the Hubnerite chlorination reactions for temperature between 750 and 850 °C, $P_{Cl_2} = 35$ kPa; Cl_2(g)–Ar(g) flow = 4 L h^{-1}, and initial mass = 1 mg.

The activation energy for the chlorination reaction can be obtained from the slope of the plot $\ln k$ vs. T^{-1}, and, as expected by the good correlation coefficient obtained in the fitting, the corresponding value of 196 ± 5 kJ mol^{-1} is in a good agreement with the previous value obtained in Section 4.3.2.3.

From Eq. (24) the following relationship between conversion and time was established:

$$f(\alpha) = 1 - (1-\alpha)^{1/3} = k_0 \cdot B \cdot \exp\left(\frac{-Ea_{(aparent)}}{RT}\right) \cdot P_{Cl_2}^{x} \cdot t \tag{25}$$

where $1-(1-\alpha)^{2/3}$ is the $f(\alpha)$ function that describes the geometric evolution of the reacting solid, Ea is the apparent activation energy, P_{Cl_2} is the chlorine partial pressure, and x is the exponent of potential function of the chlorine partial pressure dependence. The $k_0 \cdot B$ product was determined by the intersection of the curve of the linear fit from the plot: $-\ln t_i$ vs. $\ln(P_{Cl_2(g)})$ with the "y" axis.

The corresponding conversion degree vs. time curves according to Eq. (25) are plotted in Fig. 15 together with the experimental values. It shows that a good agreement exists between experimental and calculated conversions for all temperatures.

In the preceding sections, the effects that can influence the chlorination reaction kinetics were analysed. A global apparent rate equation that includes all these parameters has been proposed for the authors. Based on these results, it is concluded that Hubnerite chlorination kinetics is under mixed control in a temperature range of 750–850 °C.

By differentiating Eq. (25) with respect to time and rearranging, the reaction rate expression also can be presented as follows:

$$\frac{d\alpha}{dt} = (1-\alpha)^{2/3} \cdot k_0 \cdot B \cdot \exp\left(-\frac{Ea_{(aparent)}}{R \cdot T}\right) \cdot P_{Cl_2}^{x} \tag{26}$$

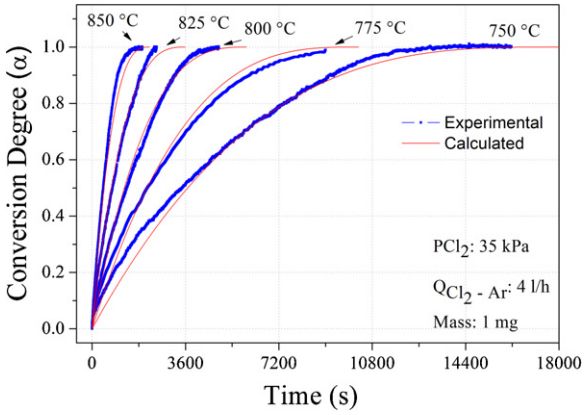

Fig. 15. Experimental conversion vs. time curves for temperatures between 750 °C and 850 °C together with calculated conversion vs. time curves according to Eq. (25).

In a future paper, the authors will present the application of a mixed control kinetic model in order to obtain the kinetic intrinsic parameters of the Hubnerite chlorination reaction.

5. Conclusions

By non-isothermal thermogravimetry, it was determined that the Hubnerite chlorination reaction begins slowly at 650 °C and increases significantly above 850 °C.

The formation of $MnCl_2$ and WO_2Cl_2 like reaction products was determined.

Mass transfer effects in the gaseous phase, like exhaustion of the reagent gas and diffusion through the boundary layer surrounding the solid sample, were analysed. It was established that the Hubnerite chlorination reaction is not affected neither by starvation (exhaustion of the reagent gas) nor by diffusion through the boundary layer (convective mass transfer) at temperatures lower than 850 °C.

Mass transfer through the sample pores was also analysed. It was determined that the Hubnerite chlorination reaction is strongly affected by this phenomenon at temperatures below 850 °C.

From the values of the rate constant calculated at different temperatures applying the contractile sphere model, an activation energy of 196 ± 5 kJ mol^{-1} was obtained.

For the experiment at 850 °C, it was found that the chlorination rate is proportional to a potential function of the partial pressure of chlorine whose exponent is around 0.85, up to a chlorine partial pressure of 35 kPa. Above 35 kPa no effect of the chlorine partial pressure on the chlorination rate was detected.

It was established that at temperatures below 850 °C the Hubnerite chlorination reaction is under mixed control. For temperatures above 850 °C the chlorination reaction is under mass transfers control.

The experimental thermogravimetric curves (α vs. t) were used to apply the contractile geometry kinetic models and it was found that the contractile sphere model achieved the best fit.

Finally, a global kinetic expression for Hubnerite chlorination reaction under mixed control was obtained.

Acknowledgements

The authors would like to thank the Agencia Nacional de Promoción Científica y Tecnológica (ANPCyT), Consejo Nacional de Investigaciones Científicas y Técnicas (CONICET), and Universidad Nacional del Comahue (UNComa) for the financial support of this work.

References

[1] G.V.K. Puvvada, R. Sridhar, V.I. Lakshmanan, Chloride metallurgy: PGM recovery and titanium dioxide production, J. Met. 55 (2003) 38–41.
[2] J.P. Bonsack, F.E. Schneider, Entrained-flow chlorination of titaniferous slag to produce titanium tetrachloride, Metall. Mater. Trans. B 32B (2001) 389–393.
[3] N. Kanari, E. Allain, R. Joussemet, J. Mochón, I. Ruiz-Bustinza, I. Gaballah, An overview study of chlorination reactions applied to the primary extraction and recycling of metals and to the synthesis of new reagents, Thermochim. Acta 495 (2009) 42–50.
[4] P.K. Jena, E.A. Brocchi, Metal extraction through chlorine metallurgy, Miner. Process. Extract. Metall. Rev. 16 (4) (1997) 211–237.
[5] F. Habashi, Handbook of Extractive Metallurgy, Wiley-VCH, New York, 1997.
[6] H.Y. Sohn, L. Zhou, The chlorination kinetics of beneficiated ilmenite particles by $CO + Cl_2$ mixtures, Chem. Eng. J. 72 (1999) 37–42.
[7] G. Fouga, D. Pasquevich, A.E. Bohé, Kinetics and mechanism of selective iron chlorination in an ilmetite ore, Trans. Inst. Mining Metall. Sect. C: Miner. Process. Extract. Metall. 116 (1) (2007) 230–238.
[8] P.K. Jena, E.A. Brocchi, M.P.A.C. Lima, Studies on the kinetics of carbon tetrachloride chlorination of tantalum pentoxide, Metall. Mater. Trans. B 32B (2001) 801–810.
[9] J.A. González, O.D. Quiroga, M. Del C. Ruiz, Kinetic study of the chlorination of gallium oxide, Metall. Mater. Trans. B 36B (2005) 445–452.
[10] K.W. Kashani-Nejad, S. Ng, R. Harris, Kinetics of MgO chlorination with HCl gas, Metall. Mater. Trans. B 36B (2005) 405–409.
[11] S.B. Kanungo, S.K. Mishra, Kinetics of chloridization of nickel oxide with gaseous hydrogen chloride, Metall. Mater. Trans. B 28 (3) (1997) 371–383.
[12] I. Nirdosh, M.H.I. Baird, S.V. Muthuswami, S. Banerjee, Coextraction of uranium and radium from ore with ferric chloride, Hydrometallurgy 10 (3) (1983) 265–283.
[13] Y. Sakamura, T. Inoue, T. Iwai, H. Moriyama, Chlorination of UO_2, PuO_2 and rare earth oxides using $ZrCl_4$ in LiCl–KCl eutectic melt, J. Nucl. Mater. 340 (2005) 39–51.
[14] V. Angelelli, Yacimientos Metalíferos de la República Argentina, Comisión de Investigaciones Científicas de la Provincia de Buenos Aires, La Plata, 1984.
[15] C.J. Menéndez, V.L. Barone, I.L. Botto, E.L. Tavani, Physicochemical characterization of the chlorination of natural wolframites with chlorine and sulphur dioxide, Miner. Eng. 20 (2007) 1278–1284.
[16] C.J. Menéndez, E.L. Tavani, E.J. Nolasco, Kinetic study of the isothermal and non-isothermal chlorination of a scheelite–wolframite concentrate with chlorine and sulphur dioxide, Thermochim. Acta 338 (1999) 103–112.
[17] C.J. Menéndez, E.J. Nolasco, E.J. Tavani, E. Pereira, Kinetic aspects of the chlorination of wolframite and of scheelite with chlorine and sulphur dioxide, Mater. Chem. Phys. 40 (1995) 273–280.
[18] S.K. Kim, The Determination of the Kinetics of Gas–Solid Reactions by the Non-isothermal Technique, Ph.D. Thesis, University of Utah, 1981.
[19] HSC 6.12 Chemistry for Windows, Aoutokumpu Research, 2007.
[20] D.R. Lide, Handbook of Chemistry and Physics, 85th ed., CRC Press Inc., FL, 2005.
[21] G.G. Fouga, G. De Micco, A.E. Bohé, Chlorination of manganese oxides, Thermochim. Acta 494 (2009) 141–146.
[22] JCPDS Joint Committee for Powder Diffraction Standards, Powder Diffraction File, International Center for Diffraction Data, Swarthmore, PA, 1996.
[23] J. Szekely, J.W. Evans, H.Y. Sohn, Gas–Solid Reactions, Academic Press, New York, 1976.
[24] A.W.D. Hills, The importance of convective mass transfer in the reduction of hematite, Metall. Mater. Trans. B B9 (1978) 121–128.
[25] W.E. Ranz, W.R. Marshall Jr., Evaporation from drops. Parts I & II, Chem. Eng. Prog. 48 (1952), 141–146, 173–180.
[26] G.H. Geiger, D.R. Poirier, Transport Phenomena in Metallurgy, Addison-Wesley, Massachusetts, MA, 1973, pp. 7–13 (chapter 1).
[27] G. Hakvoort, TG measurement of gas–solid reactions. The effect of the shape of the crucible on the measured rate, Thermochim. Acta 233 (1994) 63–73.
[28] J.P. Gaviría, A.E. Bohé, The kinetics of the chlorination of yttrium oxide, Metall. Mater. Trans. B 40B (2009) 45–53.
[29] M.R. Esquivel, A.E. Bohé, D.M. Pasquevich, Chlorination of cerium dioxide, Thermochim. Acta 398 (2003) 81–91.
[30] G. De Micco, G.G. Fouga, A.E. Bohé, The chlorination of zinc oxide between 723 and 973 K. A kinetic model, Metall. Mater. Trans. B 38B (2007) 853–862.
[31] J.H. Flynn, Thermal analysis kinetics – problems, pitfalls and how to deal with them, J. Therm. Anal. 34 (1988) 367–381.
[32] S. Vyazovkin, Computational aspects of kinetic analysis. The ICTAC kinetics project – the light at the end of the tunnel, Thermochim. Acta 355 (2000) 155–163.
[33] G. De Micco, A.E. Bohé, H.Y. Sohn, Intrinsic kinetics of chlorination of WO_3 particles with Cl_2 gas between 973 K and 1223 K (700 °C and 950 °C), Metall. Mater. Trans. B 42B (2011) 316–323.
[34] J.P. Gaviría, Modelos cinéticos de reacciones heterogéneas, Phd Tesis, Instituto Balseiro, Universidad Nacional de Cuyo, 2009.